APPLIED AND ENVIRONMENTAL MICROBIOLOGY, Mar. 1983, p. 1094–1108
0099-2240/83/031094-15$02.00/0

Vol. 45, No. 3

Diagenesis of Metals Chemically Complexed to Bacteria: Laboratory Formation of Metal Phosphates, Sulfides, and Organic Condensates in Artificial Sediments

T. J. BEVERIDGE,[1]* J. D. MELOCHE,[2] W. S. FYFE,[3] AND R. G. E. MURRAY[4]

Department of Microbiology, College of Biological Science, University of Guelph, Guelph, Ontario, N1G 2W1[1]; Petro Canada Research Laboratories, Calgary, Alberta, T2N 1N4[2]; Department of Geology[3] and Department of Microbiology and Immunology,[4] University of Western Ontario, London, Ontario, N6A 5C1, Canada

Received 20 September 1982/Accepted 15 December 1982

Cells of *Bacillus subtilis*, when suspended in a 5mM metal solution, bind metals tenaciously to their cell walls. These metal-loaded cells, when mixed with a synthetic sediment and put under laboratory conditions to simulate low-temperature sediment diagenesis, nucleate the formation of a mixed assemblage of crystalline metal phosphates, metal sulfides, and polymeric, metal-complexed, organic residues. The sequential series of diagenetic events leading to the formation of authigenic mineral phases was followed by transmission electron microscopy and energy-dispersive X-ray analysis. The minerals quartz (SiO_2) and calcite ($CaCO_3$) were employed in the synthetic sediment. Crystalline magnetite (Fe_2O_3) and elemental sulfur were added as redox buffering agents to ensure anoxic conditions. Quartz and magnetite appeared unreactive throughout the experimental conditions. Elemental sulfur interacted with the metal-loaded cells, affected both the eventual chemistry and crystal habit of the metal phosphates, and formed a variety of crystalline metal sulfides. Calcite raised the pH of the fluid phase of the sediment, which influenced phosphate mineralization and inhibited metal sulfide genesis.

There is an intricate yet delicate web of microbial interaction with the environment. One of these interactions concerns the transport of metals and their various organic derivatives throughout nature, and it is well established that a significant fraction of many metals in the hydrosphere is contained in the biomass. For example, some bacteria, such as *Thiobacillus* spp., are able to interact with and leach metals from minerals (25); sulfate reducers contribute to sulfide minerals (10), and *Spherotilis* and *Leptrothrix* spp. incorporate ferric and manganese oxides into the substance of their sheaths (1, 35); each affects metal mobility in the environment. Yet we are also accumulating evidence that most microbial surfaces are anionic (5, 6, 9, 13, 27) and consequently interact passively with available cations in the surroundings. In particular, the cell walls of *Bacillus subtilis* bind many metal species (5, 9) by means of chemical complexing with available constituent carboxylate and phosphodiester groups (8, 16, 23). Metal species which occur in minute amounts in the water column (e.g., high atomic number elements [19, 21, 26]) were especially bound in large quantities (5), and this has led us to speculate that biological polymers serve to immobilize and concentrate rare metals in nature (4). For example, although the oceans contain only 1 to 3.3 ppb soluble uranium (1 to 3.3 ng/ml) (19, 25), this could provide ca. 1.4×10^{12} kg of sedimentable uranium if efficient bioprecipitation occurred.

A significant portion of the organic matter of aquatic (both marine and freshwater) sediments consists of small colloidal aggregates which are composed of highly cross-linked heteropolymeric materials of biological origin (17). These are very resistant to degradation, and at least some of the most durable polymeric networks are of bacterial origin (15). The fate of microbial matter in the water column is a complex issue which depends on a number of factors such as biological and chemical degradation, redox potential, pH, ionic flux, etc. A light but consistent rain of bacteria and their products throughout our seas and lakes may contribute a variable proportion of their bottom sediments. These bacteria would interact with and sequester dilute metals from the aqueous phase, thereby concentrating the metals into the sediment. Here they would remain either complexed as bio-metal coordinates, or would undergo a series of microbial or chemical transformations. Eventually,

sedimentary diagenesis would either recycle the metals to the overlying water column or immobilize them in authigenic mineral phases.

The exact mechanisms and series of steps leading to low-temperature mineralization of organic-rich sediments are poorly defined, but the evidence of microfossils (32) and their organic remains (18, 31) in metalliferous sedimentary rocks makes it tempting to speculate that microorganisms have contributed to some of these processes. This report outlines experiments which have attempted to simulate low-temperature sediment diagenesis, using bacterially complexed heavy metals as the sole organic and heavy metal source. An attempt has been made to follow the steps involved and to correlate them with the complex metal-organic-sediment interrelationships which naturally occur at the hydrosphere interface, leading to the formation of authigenic phosphates and sulphides.

MATERIALS AND METHODS

Preparation of bacterial cells. *B. subtilis* (Marburg strain) was grown to exponential growth phase in 3 liters of NSMP medium as outlined previously (9). The cells were harvested by 5,000 × *g* centrifugation and were washed three times in 0.05 M *N*-2-hydroxyethylpiperazine-*N'*-2-ethane-sulfonic acid (HEPES) buffer adjusted to pH 7.2 and once in deionized, distilled water. They were then suspended in 5 mM concentrations of either $FeCl_3 \cdot 6H_2O$, $CuCl_2 \cdot 2H_2O$, $ZnCl_2$, or $UO_2(C_2H_3O_2)_2 \cdot 2H_2O$ (0.5 mg [dry weight] cells per ml of metal solution) for 10 min at 22°C, pelleted by centrifugation, washed three times with deionized distilled water, and freeze-dried under vacuum.

For each sample, the location and efficiency of metal binding were checked and recorded by the electron microscopy (EM) of unstained thin sections, using the sorbed metals as the sole electron scattering agents (9).

Preparation of synthetic sediment. "Spec pure" calcium carbonate and crystalline quartz were chosen as components for the synthetic sediments used in the diagenesis experiments. The former was chosen because of its alkalinity, whereas the latter was chosen because of its chemical inertness. Each mineral was ground in an agate mortar and sieved to less than 200 mesh. Elemental sulfur and crystalline magnetite (1-mm grains) were used as redox buffers to remove dissolved oxygen and to ensure adequately low Eh values throughout the experimental runs. All minerals were checked by powder X-ray diffractometry.

Experimental procedure for geological aging. Diagenesis experiments were carried out by mixing approximately 25 mg of dried bacterial cells, 50 mg of either elemental sulfur or magnetite, 250 mg of prepared synthetic sediment, and 0.5 ml of pure, deionized type II water (Milli-R/Q Water Purifier, pH 7.0) in a Pyrex tube (1-mm wall thickness, 6-mm bore, 1 to 1.5-ml capacity). When combinations of minerals were used in the sediment preparation, they were mixed on a 1:1 basis to the required amount. After being sealed by flame, the tubes were heated in a temperature-controlled oven at 100 ± 2°C for periods of 1, 10, 100, and 200 days. The reaction usually produced a positive pressure within each vial which was estimated to be in the order of 1 bar (100 kPa).

TABLE 1. Metal-sediment-redox buffer combinations and controls used in the artificial aging of metal-loaded cells of *B. subtilis* for 1, 10, 100,[a] and 200 days[b] at 100°C

Metal	Sediment mixture	Redox buffering agent
Uranium	SiO_2	Magnetite
	SiO_2	Sulfur
	SiO_2-$CaCO_3$	Magnetite
	SiO_2-$CaCO_3$	Sulfur
	Absent	Magnetite
	Absent	Sulfur
Copper	$CaCO_3$	Magnetite
	SiO_2	Magnetite
	SiO_2	Sulfur
	SiO_2-$CaCO_3$	Magnetite
	SiO_2-$CaCO_3$	Sulfur
	Absent	Magnetite
	Absent	Sulfur
Iron (III)	SiO_2	Magnetite
	SiO_2-$CaCO_2$	Magnetite
	SiO_2-$CaCO_2$	Sulfur
	Absent	Magnetite
	Absent	Sulfur
Zinc	Absent	Magnetite
	Absent	Sulfur
Control cells	SiO_2	Magnetite
	SiO_2-$CaCO_3$	Magnetite
	SiO_2-$CaCO_3$	Sulfur
Absent	Absent	Magnetite
Absent	Absent	Sulfur

[a] Some samples from the 1-, 10-, and 100-day runs were lost due to breakage of the Pyrex tube during heating.

[b] Not all combinations were carried through to 200 days.

A complete list of the metal-sediment-redox buffer combinations is listed in Table 1. Controls for the experiments consisted of: (i) runs employing unreacted control cells (no sorbed metal) and various sediment mixtures; (ii) runs employing the same control cells without the addition of synthetic sediment; (iii) runs employing metal-loaded cells without the addition of synthetic sediment; (iv) duplicate runs employing the alternate redox buffering agent, and (v) runs consisting solely of the redox buffering agents without the addition of either cells or sediment.

Electron microscopy. On cooling, the Pyrex tubes were carefully opened, releasing the gaseous products, and a portion of the cell-sediment mixture was removed by pipette for EM analysis. These samples were enrobed in 2% Noble agar (Difco Laboratories), dehydrated through an ethanol-propylene oxide series, embedded in Epon 812, and thin-sectioned to a thickness of approximately 60 nm. Both fixed (with 4% glutaraldehyde) and unfixed specimens were used. Sections were collected on carbon-Formvar-coated 200-mesh copper grids and examined with a Philips EM300 transmission electron microscope equipped with a goniometer stage and operated under standard conditions at 60 kV. No stains were employed for EM, relying upon the complexed metals for electron scat-

ter. Selected specimens were examined in either a Philips EM400 transmission electron microscope or a JEOL-100CX-TEMSCAN. The EM400 was fitted with a STEM attachment and a Kevex Si(Li) energy dispersive X-ray (EDX) system which allowed spot-mode analysis with a spatial resolution of 20 nm. The TEMSCAN was equipped with a similar Kevex system. Both instruments were operated at 80 kV, and count times were 200 s (the EM400 specimen-to-detector angle was 20 degrees, whereas the TEMSCAN angle was 40 degrees).

EDX spectra were obtained from both whole mounts and unstained plastic (Epon 812) embeddings which were mounted on either 200-mesh nylon grids or copper grids. Those specimens on copper grids had a characteristic copper peak at 8.05 keV. Since cells of *B. subtilis* are generally low in chlorine, the relatively large chlorine peaks (at around 2.69 keV) are considered to be due to contamination from the Epon 812 matrix. Likewise, the presence of a prominent silicon peak (at around 1.75 to 1.8 keV), regardless of the instrumentation used or the material analyzed, suggests contamination from the glassware, although biological leaching cannot be ruled out (20).

The minerals produced by the experiment were all extremely fine grained (less than 5 μm), and consequently their identification relied solely on interpretation of transmission electron microscope images supported by qualitative X-ray spot analysis. Thin sections of the crystalline products were often too electron dense to provide accurate diffraction images. However, in most cases, the crystal symmetry and chemical analyses provided sufficient information for tentative identification.

Both X-ray diffraction analysis, using an 11-cm Debye-Sherrer camera and standard scanning electron microscope analysis were attempted. However, the results proved inconclusive due to the high matrix-to-cell ratio and the extremely fine nature of the authigenic constituents.

pH analysis. The pH of the reaction fluid was checked for 19 selected samples covering a wide range of metal-sediment-redox buffer combinations heated for 100 and 200 days (see Table 3). All pH analyses were carried out in a nitrogen atmosphere to prevent oxidation of dissolved constituents. On opening the tubes, a small quantity of fluid was blotted onto three different pH indicator papers having overlapping ranges graduated into 0.3 pH units. This enabled the pH to be approximated within ± 0.2 pH units.

RESULTS

Organic diagenesis. Although all reaction vessels were sealed under atmospheric pressure, those containing bacterial cells usually developed pressure (estimated to be between 0.5 and 1.0 bar [50 to 100 kPa]) after 10 days of incubation at 100°C. Generally, the pressure increased with the length of the incubation period. Also, the fluid phase in those tubes containing bacteria developed a yellow color which was independent of the presence or nature of test metals, sediment, or redox buffering agent. In natural surface waters, yellow colorations are commonly due to the presence of dissolved, complex carboxylic acids, phenols, and amines (W. J. Maier, L. E. Conroy, and C. T. Anderson, Proceedings of the International Symposium on Geochemistry of Natural Waters, 1975. p. 22, Burlington, Canada). Presumably, the discoloration of the test fluids was a consequence of the synthesis of soluble organics during the thermal degradation of the bacterial cells. Since the volume of the test fluid was so small (≤0.1 ml), specific organic analyses were not possible.

The contents of each reaction vessel were sampled and processed for the electron microscopy of thin sections. This allowed us to follow structural changes in the bacteria during diagenesis. Since no stains were used on these specimens other than the metal which was originally sorbed to the cells (Fig. 1), electron scattering profiles allowed us to monitor the migration of metal during the experiment. The quantities of bound metal have been previously published and can be found in references 5 and 9. Energy dispersive X-ray analyses (EDX) analyses of select areas within each specimen provided compositional data during the experiment. A listing of the results of the experimentation can be found in Table 2, and a survey of our observations by EM is seen in Fig. 1 to 23.

In general, the observed sequence of events was as follows: (i) loss of structure of the bacterial wall and its subsequent mineralization (extracellular phosphate crystallization—see Fig. 2, 3, and 5); (ii) release of some of the wall-bound metal and its subsequent migration (at least some migrated into the cytoplasm [Fig. 3, 5, and 8]); (iii) condensation and polymerization of the cytoplasmic contents and their mineralization (intracellular phosphate crystallization—see Fig. 4, 8, 12, 13, 14, and 18); (iv) continued condensation, polymerization, and mineralization of the organics, often resulting in the loss of basic cell shape (Fig. 8, 9, and 19); and (v) intense polymerization of metal-complexed organics and pronounced organic-metal phosphate (or metal sulfide) interaction leading to recrystallization (Fig. 15–17, 19, 20).

These reactions were followed by EDX analyses which confirmed that the eventual authigenic mineral phase contained the metal which was originally supplied by the bacteria. When magnetite was used as a redox buffer, there was no detectable iron in the mineral phase (i.e., the magnetite had not been leached [Fig. 3 to 7]). However, the use of the elemental sulfur as a redox buffer usually produced crystalline metal sulfide as an end product (Fig. 16, 17, and 21–23).

Often the cells occurred in large aggregates of ca. 25 to 50 μm in diameter (presumably due to their reduced wettability after freeze-drying). Mineralization occurred first at the periphery of

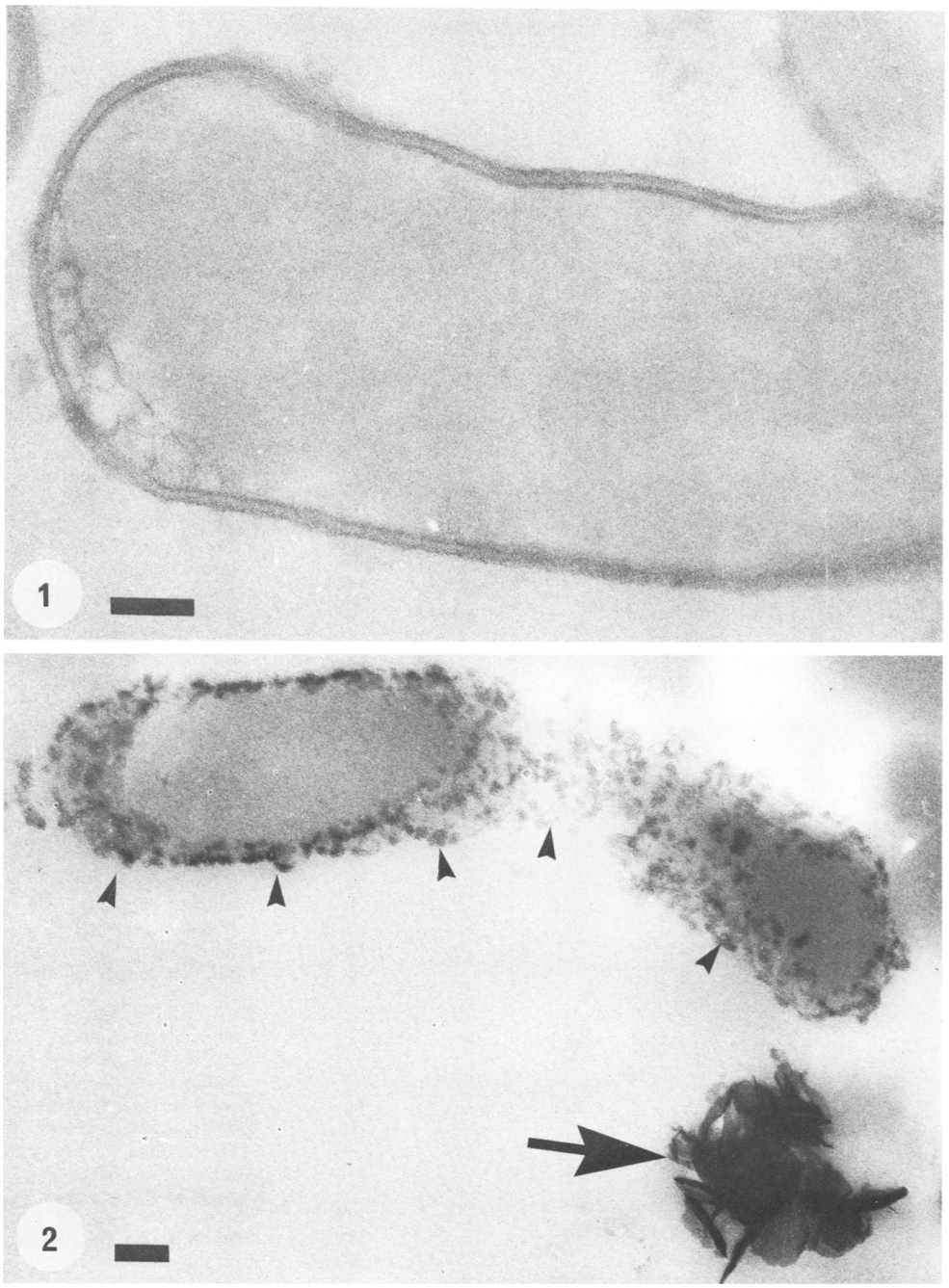

FIG. 1 and 2. (1) Thin section of a uranium-loaded *B. subtilis* cell. In this and in all other micrographs, no stains other than the sorbed metal were used on the material. Most of the uranium has partitioned into the cell wall. (2) Thin section of control cells (no sorbed metal) after artificially aging with magnetite at 100°C for 100 days. Note the incipient crystallization of the walls (small arrows) and formation of large platy aggregates of a "probable" phosphate mineral (large arrow). Bars = 100 nm.

these clumps and proceeded inwards towards the center. With these samples, the sequence of events leading to mineralization could be followed by examining select areas throughout the aggregate. After 200 days of reaction, mineralization was usually complete. Highly electron-dense polymeric organic residues, together with their prominent EDX metal peaks (Fig. 9, 11, 16,

TABLE 2. Mineralization during experiments[a]

Metal[b]	Sediment[c]	*B. subtilis*[d]	Redox buffer[e]	Mineralization
Controls (no sorbed metal)	Q	−	−	
	Q	−	M	
	Q	−	S	
	Q	+	−	Phosphate microcrysts
	Q	+	M	Phosphate microcrysts
	Q	+	S	Phosphate microcrysts
	C	−	−	
	C	−	M	
	C	−	S	
	C	+	−	Phosphate microcrysts[f]
	C	+	M	Phosphate microcrysts[f]
	C	+	S	Phosphate microcrysts[f]
Uranium	−	+	M	Uranium phosphate microcrysts
	−	+	S	Uranium phosphate microcrysts; polymeric uranium-organic sulfide residues
	Q	+	M	Uranium phosphate microcrysts
	Q	+	S	Uranium phosphate microcrysts; polymeric uranium-organic sulfide residues
	Q + C[g]	+	M	Uranium phosphate microcrysts[f]
	Q + C[g]	+	S	Uranium phosphate microcrysts[f]; polymeric uranium-organic sulfide residues
Copper	−	+	M	Phosphate microcrysts[h]
	−	+	S	Dominant copper sulfides + traces of phosphate microcrysts[h]
	Q	+	M	Phosphate microcrysts[h]
	Q	+	S	Dominant copper sulfides + traces of phosphate
	Q + C[g]	+	M	Minimal phosphate microcrysts[f]
	Q + C[g]	+	S	Dominant copper sulfides[f]
Zinc	−	+	M	Phosphate microcrysts[h]
	−	+	S	Dominant zinc sulfides + traces of zinc phosphate microcrysts
	Q	+	M	Phosphate microcrysts
	Q	+	S	Dominant zinc sulfides + traces of phosphate microcrysts
	Q + C[g]	+	M	Minimal phosphate
	Q + C[g]	+	S	Dominant zinc sulfides
Iron	−	+	M	Iron phosphate microcrysts
	−	+	S	Iron phosphate microcrysts

[a] Due to limitations of time and space, not all combinations were run. Those chosen were intuitive and of most interest to the authors.

[b] Metal which was sorbed to bacterial cells.

[c] Q, Quartz (SiO_2); C, calcite ($CaCO_3$).

[d] −, Bacteria absent; +, bacteria present.

[e] M, Magnetite; S, elemental sulfur.

[f] No calcium was detected associated with these microcrysts.

[g] Calcite was added as a pH buffer, and the extent of phosphate mineralization was reduced as a consequence of the higher pH.

[h] Phosphate mineralization was reduced from that seen in the uranium and iron experiments.

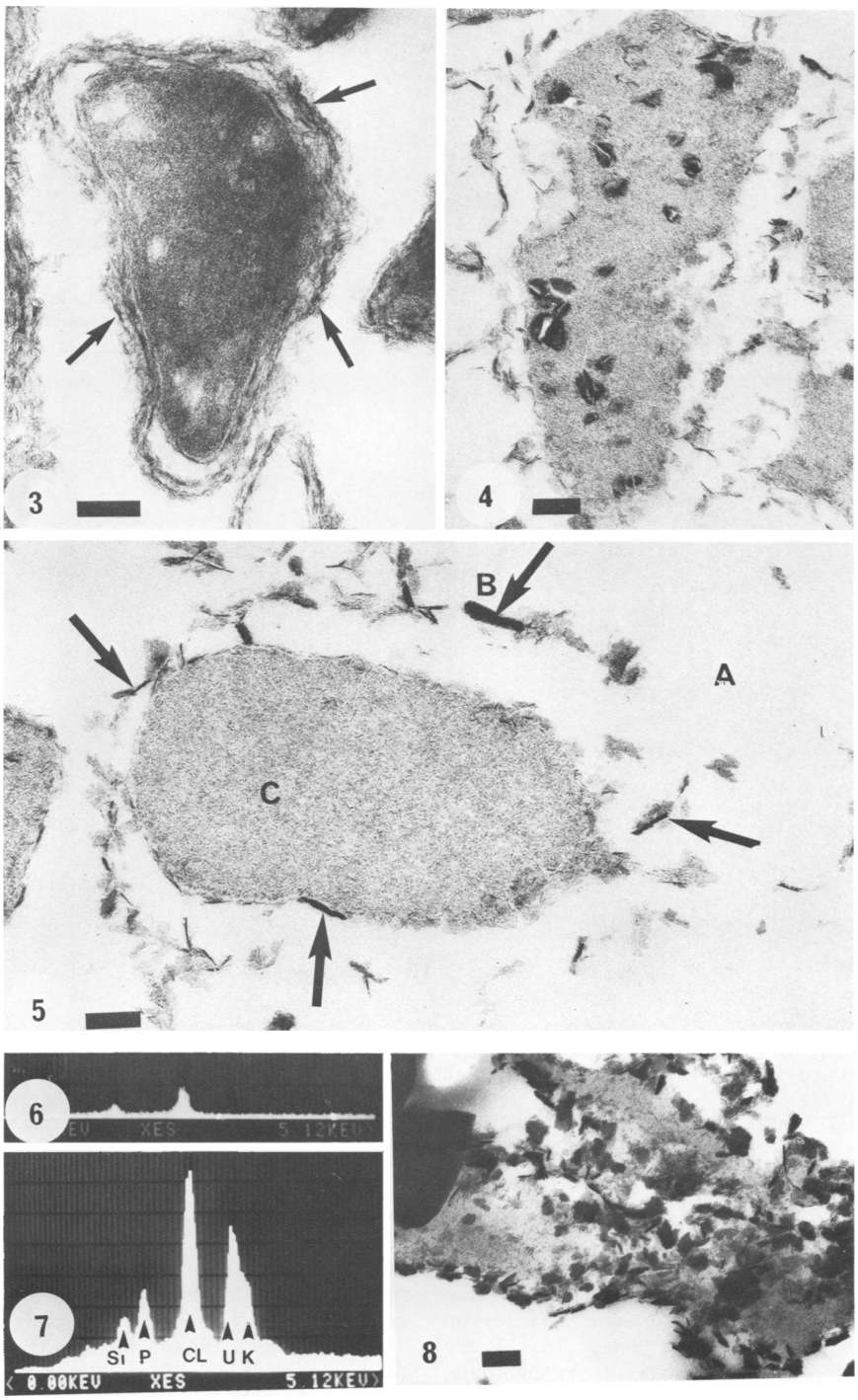

FIG. 3–8. (3) Thermal degradation of uranium-loaded cells in quartz with magnetite after 1 day. The wall has begun crystallization; arrows point to developing microcrysts. (4) Same as Fig. 3 but after 10 days. Platy phosphate microcrysts are found in the wall and cytoplasm. (5) Same as Fig. 4. This cell was used to generate the EDX spectra in Fig. 6 and 7. Large arrows point to a few of the microcrysts. (6) EDX spectrum of area A (the plastic) in Fig. 5. (7) EDX spectrum of area B (the wall microcrysts) in Fig. 5. The cytoplasm (area C) has a similar spectrum, but the quantities of the elements were reduced. (8) A clump of cells after 100 days. The crystallization is intense. Bars = 100 mm.

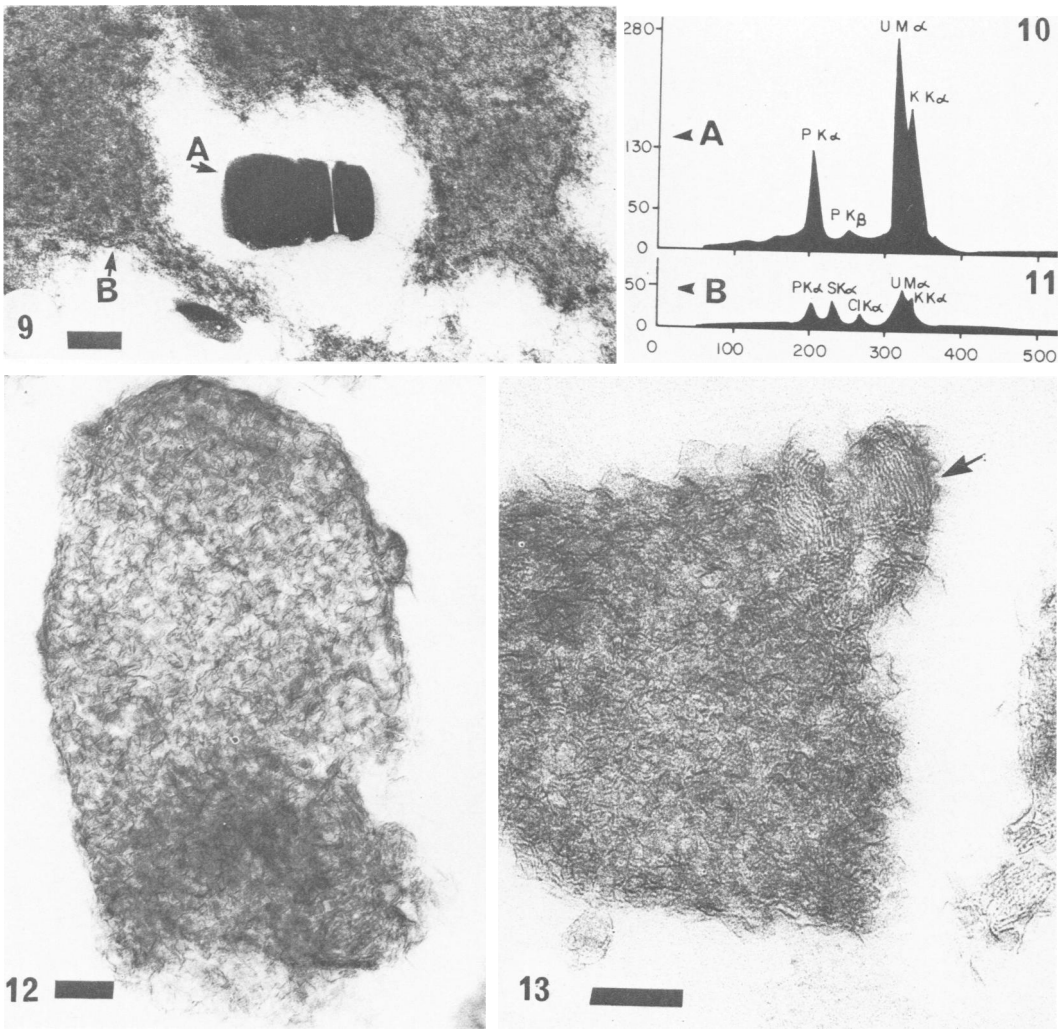

FIG. 9–13. (9) Thermal degradation of uranium-loaded cells aged for 200 days with sulfur as a redox buffer. Uranium phosphate crystallization (note the perfect micacaeous, basal 001? cleavage of the electron dense microcryst) and sulfurous organic condensates (fibrillar material) are clearly seen. Areas A and B have been analyzed by EDX. (10) EDX spectrum of the area labeled "A" in Fig. 9. (11) EDX spectrum of the area labeled B in Fig. 9. (12) Thermal degradation of a uranium-loaded cell aged in quartz and calcite with a magnetite redox buffer for 10 days. Tiny uranium phosphate microcrysts are seen throughout the cell. (13) Same as Fig. 12 but aged for 1 day. Incipient polymerization (arrow) and intracellular crystallization are shown. Bars = 100 nm.

19, 21) provide strong support for the synthesis of insoluble organic-metal complexes during diagenesis. Diffuse electron opaque surfaces on crystalline phosphate (Fig. 9, 15, 18, 20) are interpreted as thin coatings of organic-metal residues which have adsorbed to the crystal faces.

Apart from the mineralization and loss of cell wall structure, cellular degradation appeared less pronounced in runs employing iron-, copper-, and zinc-loaded cells. Degradation was most apparent by the formation of phosphate microcrysts (Fig. 20), of large spheroidal structures associated with framboidal metal sulfide (which are interpreted as organic colloids [Fig. 15]), of granular sulfide spherules (Fig. 19), and of the incipient polymerization of cytoplasmic material (Fig. 9 and 18). Tests carried out with unreacted control cells yielded similar results; after aging, the loss of cell wall structure and incipient crystallization of phosphate mineral occurred (Fig. 2).

Phosphate mineralization. Thermal degradation of uranium-loaded cells resulted in the crys-

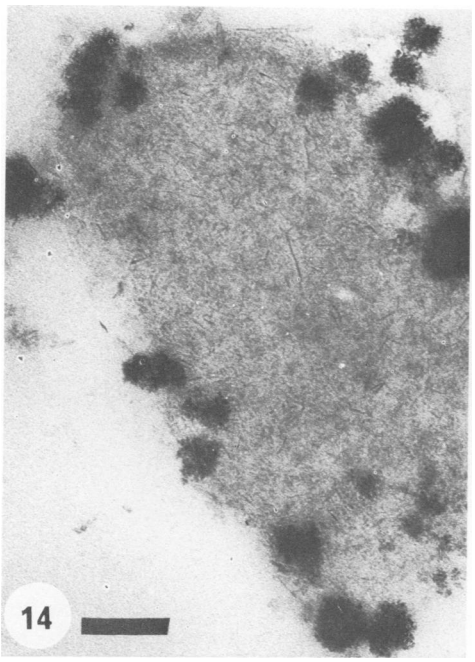

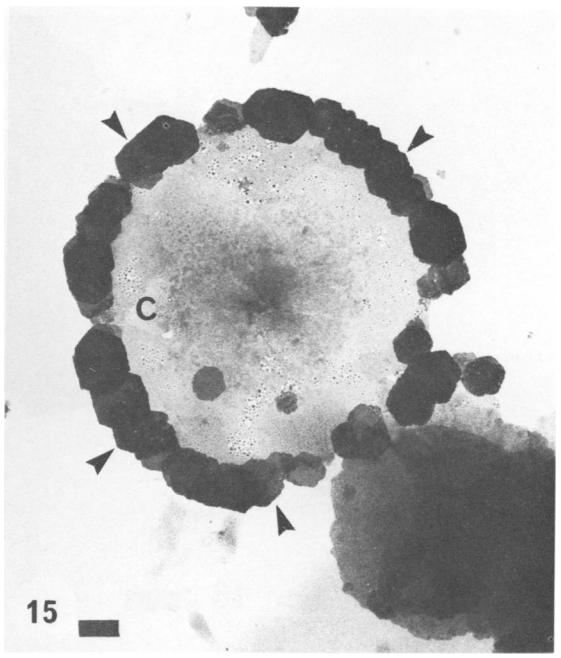

FIG. 14–15. (14) Same as Fig. 12, but elemental sulfur instead of magnetite is the redox buffer. Aging time is 10 days. Extracellular uranium phosphate microcrysts with electron-dense organic coatings can be seen. (15) This preparation contained copper-loaded cells, quartz, and sulfur and was aged for 10 days. A mixed assemblage of isolated euhedra, framboids, and crystalline aggregates was produced. Seen here is an example of authigenic copper sulfide production; copper sulfide microcrysts (arrows) are arranged around electron translucent, colloidal organic material (C), and this image is interpreted to indicate incipient framboid development. Bars = 100 nm.

tallization of a phosphate mineral in all experimental runs independent of the nature of the sediment or redox buffering agent used (Table 2). Mineralization began in the bacterial wall as fine acicular or tabular microcrysts about 60 nm in length (Fig. 3 and 5), and these grew in size until at the 200-day stage, phosphate needles $\geq$10 μm were common. EDX spectra (Fig. 7 and 10) for all crystal stages were similar, and these results plus the crystal "habit" (Fig. 9) are consistent with those characteristics of meta-ankoleite, a hydrated phosphate mineral of $K_2(UO_2)(PO_4)_2 \cdot 6H_2O$ chemistry.

Similar microcrysts were observed in a number of runs involving copper-loaded cells (Fig. 18) and control cells (Fig. 2). Although no extensive EDX analyses were done on these specimens, their crystal form and close association with the bacterial cells resembled the potassium uranium phosphate assemblages and suggested minor phosphate mineralization.

Artificial aging of iron-loaded cells in the presence of sulfur redox buffer resulted in the synthesis of iron phosphate as isolated hexagonal plates or aggregates composed of a mixture of fine microcrysts and elemental sulfur (Fig. 20, 22, 23). The platy habit and hexagonal symmetry of the iron phosphate suggests cacoxenite, a hydrated ferric phosphate of $Fe_9(PO_4)_4(OH)_{15} \cdot 18H_2O$ chemistry.

Sulfide mineralization. Metal sulfides were synthesized in all experimental runs where copper- or zinc-loaded cells were aged in the presence of elemental sulfur without calcium carbonate (calcite) in the system. Copper sulfides occurred in a mixed assemblage of framboids, crystalline aggregates, and discrete euhedral microcrysts (Fig. 15–17). The sulfide euhedra were frequently associated with electron transparent colloidal material which could be of organic nature (Fig. 15). Continued aging for 200 days produced a dramatic increase in both crystal size and crystal form (compare Fig. 16 and 17). EDX analyses of these sulfides indicated that these were pure phases, although the cubic form contained small amounts of iron. The hexagonal form is most probably covellite (CuS), although low-temperature, hexagonal chalcocite (Cu_2S) cannot be ruled out (12). The cubic form is consistent with the characteristics of digentite [$(Cu, Fe)_9S_5$] which is stable at temperatures above 83°C (12).

Zinc sulfide was formed from zinc-loaded cells, and, like the copper sulfides, was present

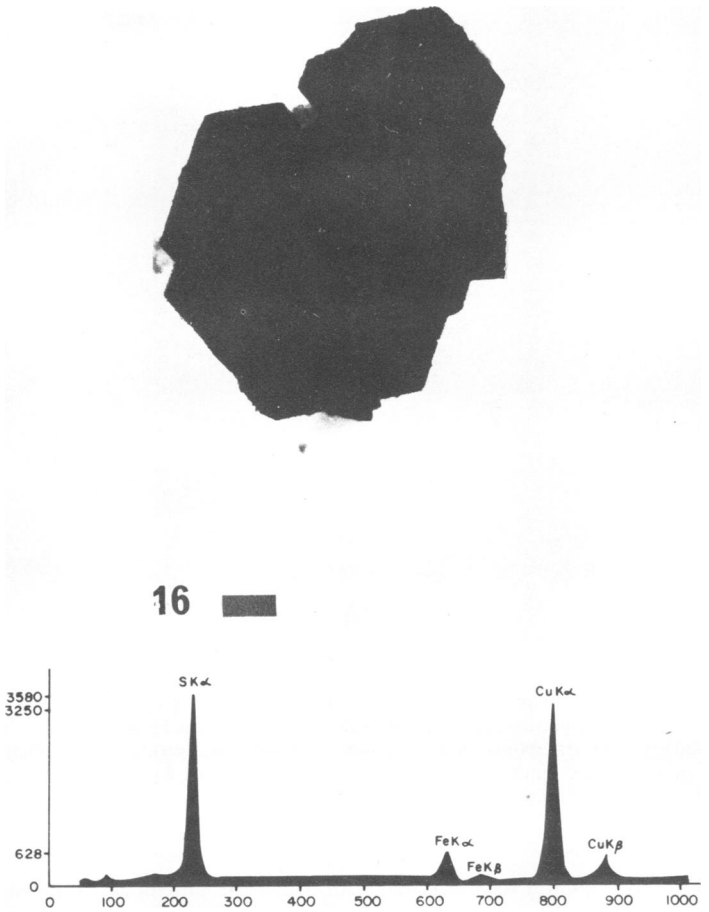

FIG. 16. Same as Fig. 15, but aged for 200 days. A large hexagonal crystal aggregate of copper sulfide [either covellite (CuS) or chalcocite (Cu_2S)] is shown at top, and its EDX spectrum is shown below. Bar = 100 nm.

in a variety of crystalline forms resembling those shown in Fig. 15 to 17. However, the bulk of the zinc sulfide occurred as electron-opaque granules and spherules (hollow granules) which were intimately associated with the bacterial cells (Fig. 19). With progressive aging, the size of the granular spherules increased at the expense of the isolated granules. It therefore seemed that these spherules grew by accretion of the isolated granules. It is possible that the electron-transparent zone in the center of each spherule is an organic phase. The sites of development observed by electron microscopy indicate that the bacterial surface (presumably the wall) is necessary for their growth, and EDX confirmed that the crystalline and granular forms were pure zinc sulfide phases (Fig. 21).

Conditions of product formation. The pH and ΔpH values of 19 selected experiments are shown in Table 3, together with the corresponding metal, sediment, redox buffer, and initial pH values. The final pH values of the fluid phase varied from 6.8 to 6.9 and 4.5 to 5.3, depending on whether calcium carbonate (calcite) was available as a pH buffering agent. The ΔpH values were fairly consistent for all runs, ranging from 1.7 to 2.5 pH units, regardless of the nature of the constituents or initial pH. No attempt was made to measure redox potentials since the fluid volumes were too small. However, in runs employing elemental sulfur as a redox buffering agent, a strong smell of hydrogen sulfide was detected when the vials were opened, indicating a low redox potential in these runs.

In general, organic degradation and phosphate formation were most pronounced in runs using uranium-loaded cells. In these experiments, the bacteria degraded most rapidly at the more neutral pH values (6.8 to 6.9), with the organic residues polymerizing most intensely in the presence of hydrogen sulfide. Phosphate formation correlated well with cellular decomposition, but aggregation and recrystallization of the potassium-uranium-phosphate were most intense

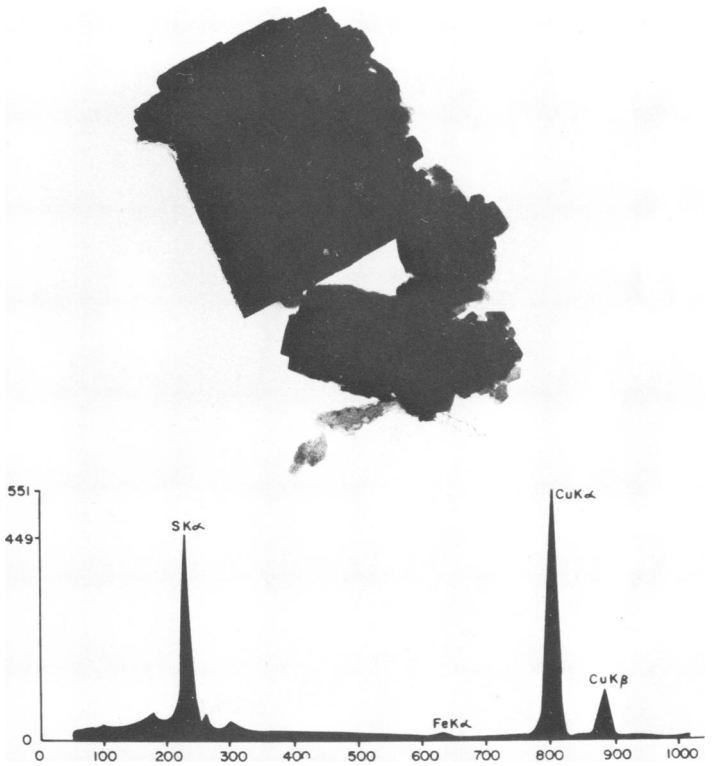

FIG. 17. Same preparation as Fig. 15, but a cubic form of copper sulfide, digentite [$(Cu,Fe)_9S_5$], is shown (EDX spectrum below).

in the absence of calcite (i.e., at the lower pH values). All copper and zinc sulfides formed at the low pH values. The lower degree of phosphate mineralization in the copper and zinc experiments suggested that highly electropositive metallic cations were a prerequisite for intense phosphate formation. Appearances suggested that the uranyl cation may have more actively catalyzed the breakdown of native cellular polymers and thus promoted the release and subsequent precipitation of organic phosphate.

DISCUSSION

The surfaces of most types of cells are highly anionic, and bacterial cells are no exception. Those of *B. subtilis* certainly react with and bind substantial amounts of metal from aqueous solution and have presented a good model system to study the binding characteristics (5, 9). We have attempted to equate these results, in a general way, to the contribution we can expect of biological polymers in nature to the mobility and migration of metals throughout the environment. We envision a light but constant rain of these polymers throughout natural bodies of water which would concentrate metals into the sediment. Here the more durable metallo-organopolymers would undergo a series of biological and geochemical degradations until mineralization was completed and a low-temperature metamorphic horizon was produced. We would expect the less durable polymers to exchange metallic ions with their more durable neighbors, thereby making possible high concentrations which could inhibit degrading enzymes. It is difficult to extrapolate the *B. subtilis* model system to a sediment environment unless experiments which mimic the environmental situation are employed. Clearly, actual experiments outside the laboratory in natural sediments would be difficult to monitor and to control. Accordingly, we had set up a series of small-volume sediment situations in the laboratory which could be controlled and accurately monitored. The only heavy metal available in each of the experimental vessels during diagenesis was that which was bound to *B. subtilis* cells.

The experiments reported here conclusively demonstrate that, given the correct conditions, organic polymers can be involved in authigenic mineralization during low-temperature diagenesis. In fact, our results indicate that the bacterial cells actively nucleated the mineralization proc-

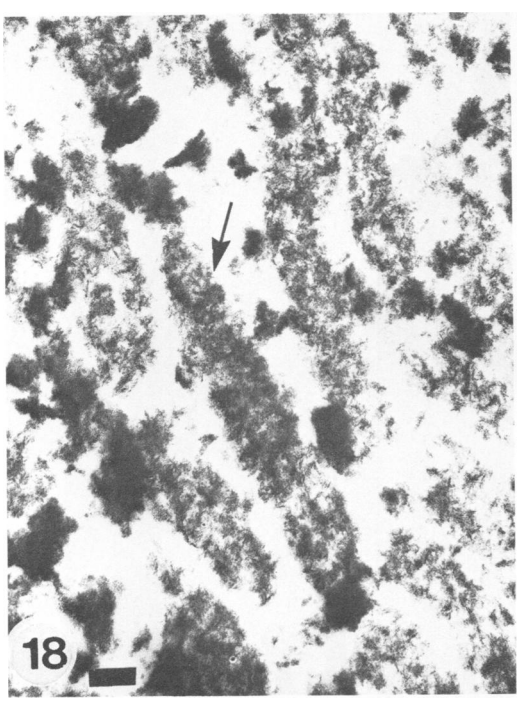

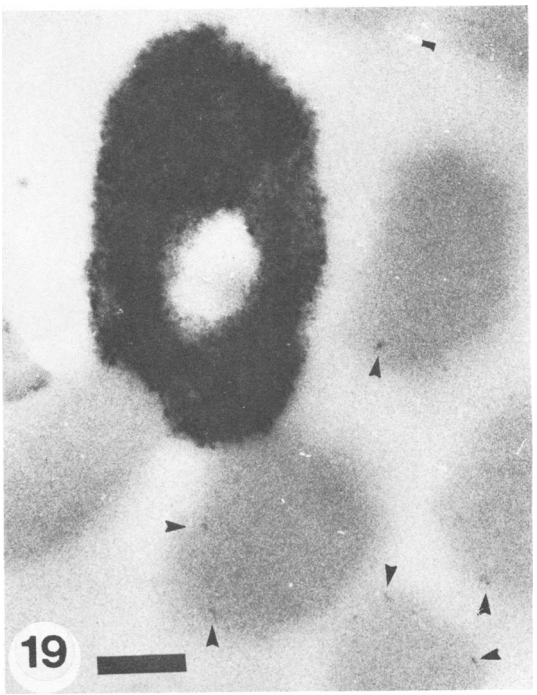

FIG. 18–20. (18) This preparation is copper-loaded cells in calcite with magnetite as the buffer and has been aged for 100 days. The cell walls have been lost, and there is intense crystallization within the cytoplasm. Even though there has been intense intracellular phosphate mineralization and condensation of organic matter, the basic shape of the cells remains intact (the arrow points to a single cell). (19) Thermal degradation of zinc-loaded cells aged with elemental sulfur for 200 days. Traces of intracellular granular sulfide mineralization are seen (small arrows), but most conspicuous are the large granular spherules of zinc sulfide which are developing at the cell periphery. (20) Thermal degradation of iron-loaded cells aged with elemental sulfur for 10 days. Coarse, electron-dense aggregates of platy iron phosphate microcrysts and elemental sulfur are shown. Bars = 100 nm.

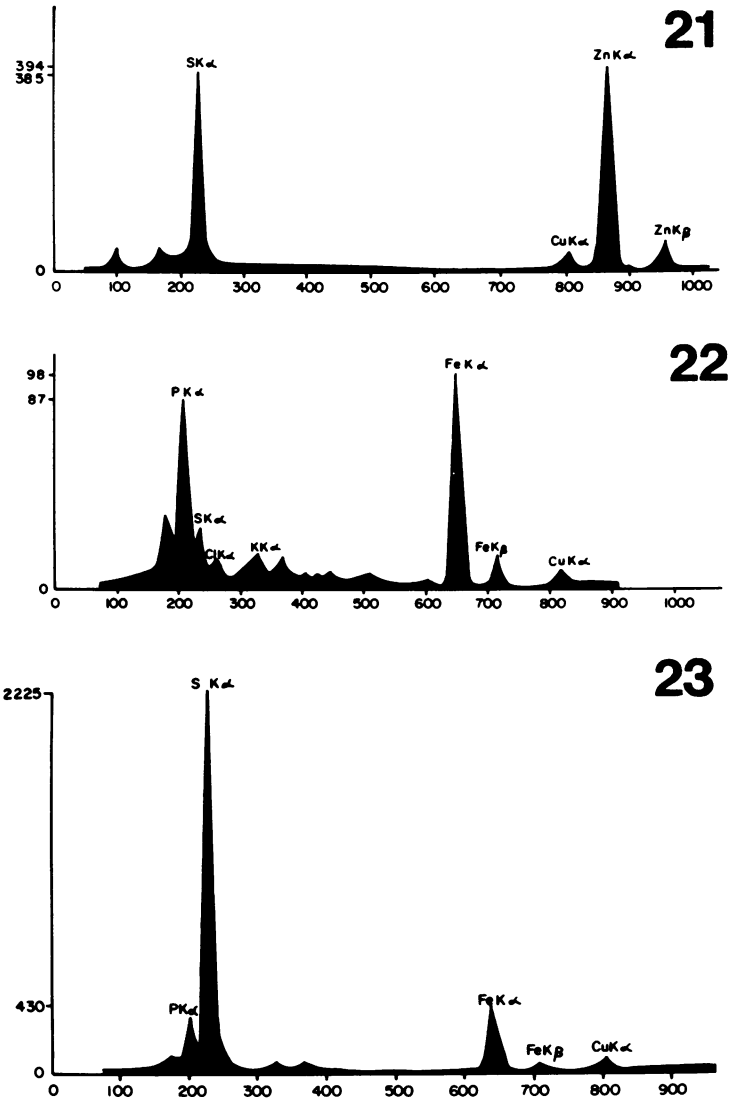

FIG. 21–23. (21) EDX spectrum of a spherule as seen in Fig. 19. (22) EDX spectrum of a hexagonal plate from the same preparation as Fig. 20, showing it to be an iron phosphate mineral. (23) EDX spectrum of the crystalline aggregate at the left ("A") of Fig. 20. It is mostly elemental sulphur with traces of an iron phosphate mineral.

ess and provided a major source of phosphorus for the production of phosphate minerals. Presumably, at the same time, the organic carbon of the cells was either highly polymerized into insoluble carbonaceous residues (commonly termed kerogen), or it was mineralized to carbon dioxide or carbonate ions and incorporated into a crystal phase. Unfortunately, carbon cannot be detected by the EDX analysis techniques used in this study and consequently, it could not be monitored under our experimental conditions.

Although carbonate fluorapatite and carbonate hydroxyapatite comprise more than 99% of the phosphorus minerals in marine sediments, the question of apatite formation during diagenesis remains unresolved. It must depend on a number of complex energy relationships (28). Like carbonate minerals, phosphate formation is commonly considered a pH phenomenon which is controlled by the partial pressure of carbon dioxide in the sediments, with apatite being the dominant phase at pH 7.1 to 7.8 (11, 22).

Our experiments contained bacteria as the sole source of phosphorus. It was present in the form of organic phosphate in the nucleic acids

TABLE 3. pH analyses for selected metal-sediment-redox buffer combinations artificially aged for 100 and 200 days at 100°C

Metal	Sediment mixture	Redox buffer	Time (days)	Initial pH	Final pH	Δ pH
Uranium	SiO_2	Sulfur	200	7.0	4.8	2.2
	Absent	Magnetite	200	7.0	5.0	2.0
Copper	SiO_2	Sulfur	200	7.0	4.5	2.5
	SiO_2	Magnetite	200	7.0	5.3	1.7
	SiO_2	Magnetite	100	7.0	5.0	2.0
	SiO_2-$CaCO_3$	Sulfur	200	9.0	6.8	2.2
	SiO_2-$CaCO_3$	Sulfur	100	9.0	6.8	2.2
	SiO_2-$CaCO_3$	Magnetite	200	9.0	6.8	2.2
	SiO_2-$CaCO_3$	Magnetite	100	9.0	6.8	2.2
Zinc	Absent	Sulfur	200	7.0	4.8	2.2
	Absent	Magnetite	200	7.0	5.0	2.0
	Absent	Magnetite	100	7.0	4.5	2.5
Iron	Absent	Magnetite	100	7.0	4.5	2.5
Control cells	SiO_2	Magnetite	200	7.0	5.0	2.0
	SiO_2	Magnetite	100	7.0	5.0	2.0
	SiO_2-$CaCO_3$	Sulfur	200	9.0	6.9	2.1
	SiO_2-$CaCO_3$	Sulfur	100	9.0	6.8	2.2
	SiO_2-$CaCO_3$	Magnetite	200	9.0	6.8	2.2
	SiO_2-$CaCO_3$	Magnetite	100	9.0	6.8	2.2

(both RNA and DNA), in the phospholipids (of membranes), and in the teichoic acids (of the cell walls). In fact, the phosphodiester groups of the bacterial walls were one of the major sites of the bound metal of metal-loaded bacteria (8). Approximately 6% of the dry weight of these cells was phosphate (T. Beveridge, unpublished data). Clearly, phosphate mineralization occurred during our experiments; this was most pronounced in the mildly acidic range. The apparent absence of calcium in the phosphates precipitated in the presence of calcite indicated either that lower pH values inhibit apatite formation or that the kinetics of its formation were too slow to have been realized in a short-term study. If apatite is inhibited by low pH, then the availability of suitable metal ions may be a critical factor in the formation of less complex metal phosphate compounds.

The aqueous chemistry of uranium is complex and is unlike that of lower atomic number metals (36), but free uranyl ion is readily coordinated to available anionic sites on biological polymers (5, 7, 8, 16). Uranium frequently demonstrates a marked positive correlation with phosphorus in modern marine sediments and fine-grained sedimentary rocks (3, 33). Marine phosphorites can contain 190 ppm uranium (190 μg/ml) (38). In organic-rich phosphatic shales, uranium is typically associated with the phosphate phase, whereas in phosphate-deficient shales, the uranium is retained by the organic phase (39). The stability of the organically complexed uranium throughout diagenesis must, to a large extent, be affected by the formation of authigenic phosphate minerals; this, in fact, has been confirmed by our experiments.

The low temperature relationships involved in the formation of sulfide minerals are not well defined. Several studies have suggested the importance of metal-organic complexes during their formation, but the partitioning of the metal to the sulfide phase most probably depends on the stability of the metal-organic compound (29, 37). Clearly, in our system, sulfide production is intimately associated with the bacterial cells and the metal which is coordinated to them. To our knowledge, this is the first instance that metal sulfide framboid production has been definitely correlated to biological material since these bacterial cells nucleated their development during the experiments.

Clearly, we must be careful in our extrapolation of these laboratory results when we attempt correlation with conditions prevailing in a natural system. However, several lines of evidence exist to support a close correlation. Organics and metal sulfides commonly exhibit close association with phosphate in fine-grained sedimentary rocks (40) and, as previously mentioned, the correlation of uranium and phosphate contents in marine sediments is well documented. The preservation of "fossilized" bacterial cell membranes as metal-organic complexes within 7,000-year-old sediments from the Black Sea, Lake Tanganika, and German oil shale (14, 15) provide compelling evidence for natural, heavy-metal sequestering by bacterial walls. "Fossilized" bacterial cells and organic coatings which are intimately associated with metal sulfide

framboids have been described from a number of organic-rich sedimentary rocks (14, 24). Recent evidence definitely promotes a bacterial origin for some phosphate accumulations. "Fossilized" bacilli have been described in freshly fractured late-Pleistocene to Holocene phosphatic nodules (30).

Numerous reports exist which indicate that microorganisms have been instrumental in the genesis of many ancient sedimentary rock types (2, 15, 18, 31, 37). In fact, organically walled structures (microfossils?) have been described in sedimentary rocks as old as 3.8×10^9 years (18, 34). The presence of bona fide fossilized bacteria has been extensively documented in cherts $<2 \times 10^9$ years old, but they become rarer and less diverse in morphology in the appropriate rocks older than that. The recognition of bacterial cells from nondescript organic residues in many sedimentary rocks is an arduous task because of simple morphology, poorer preservation relative to higher organisms, and the limited range of embedding rocks (i.e., cherts). Only EM affords the high resolution required to follow mineralization of individual bacteria and their component parts. At present, there are numerous reports in the literature of fossilized microorganisms, but most studies are at the optical level of the light microscope. Using EM, we have outlined some of the mineralization processes which contribute to the preservation of microbial cells in sedimentary rock.

Low-temperature diagenesis must occur through a series of closely related and interdependent chemical events. The study reported in this paper provides compelling evidence for the direct involvement of organic matter in the formation of late-stage diagenetic phosphate and sulfide minerals. It provides a logical immobilizing step for metal which has been chelated and sedimented by biological particulates within the natural water column. Since the dominant processes leading to the formation of phosphates and sulfides in this study were primarily governed by low-temperature reactions, it is likely that the abiotic formation of similar phases in nature can proceed at temperatures well below 100°C if given sufficient time. Given this view, some components of the organic fraction of a sediment stimulate and quicken mineral authigenesis.

ACKNOWLEDGMENTS

We express appreciation to the Natural Sciences and Engineering Research Council of Canada and the Medical Research Council of Canada for providing T.J.B., W.S.F., and R.G.E.M. with operating funds for this research. T.J.B. is grateful to the Department of Microbiology, University of Guelph, for the funds to support the EM 300.

We are indebted to M. Stewart, MRC Laboratory of Molecular Biology, Cambridge, England, for the EDX of 10-day-old phosphate microcrysts.

LITERATURE CITED

1. **Ali, S. H., and J. L. Stokes.** 1971. Stimulation of heterotrophic and autotrophic growth of *Sphaerotilus discophorus* by manganese ions. Antonie van Leeuwenhoek J. Microbiol. Serol. **37**:519–528.
2. **Banghoorn, E. S., and S. A. Tyler.** 1965. Microorganisms from the gunflint chert. Science **147**:563–577.
3. **Baturin, G. N.** 1973. Uranium in the modern sedimentary cycle. Geochem. Int. **10**:1031–1041.
4. **Beveridge, T. J.** 1977. The interaction of metals in aqueous solution with bacterial cell walls from *Bacillus subtilis*, p. 975–987. *In* W. E. Krumbein (ed.), Environmental biogeochemistry and geomicrobiology, vol. 3. Ann Arbor Science Publishers, Inc., Ann Arbor, Mich.
5. **Beveridge, T. J.** 1978. The response of cell walls of *Bacillus subtilis* to metals and to electron microscopic stains. Can. J. Microbiol. **24**:89–104.
6. **Beveridge, T. J.** 1981. Ultrastructure, chemistry and function of the bacterial wall. Int. Rev. Cytol. **72**:229–317.
7. **Beveridge, T. J., and S. F. Koval.** 1981. Binding of metals to cell envelopes of *Escherichia coli* K-12. Appl. Environ. Microbiol. **42**:325–335.
8. **Beveridge, T. J., and R. G. E. Murray.** 1980. Sites of metal deposition in the cell wall of *Bacillus subtilis*. J. Bacteriol. **141**:876–887.
9. **Beveridge, T. J., and R. G. E. Murray.** 1976. Uptake and retention of metals by cell walls of *Bacillus subtilis*. J. Bacteriol. **127**:1502–1518.
10. **Bubela, B., and J. A. McDonald.** 1969. Formation of banded sulphides: metal ion separation and precipitation by inorganic and microbial sulphide sources. Nature (London) **221**:465–466.
11. **Chauhan, D. S.** 1979. Phosphate bearing stromatolites of the precambrian Aravalli phosphate deposits of the Udaipur region: their environmental significance and genesis of phosphorites. Precambrian Res. **8**:95–126.
12. **Craig, J. R., and S. D. Scott.** 1974. Sulphide phase equilibria; the Cu-S system, p. 58–65. *In* P. H. Ribbe (ed.), Sulphide mineralogy. Mineral Society of America Short Course Notes VI.
13. **Cutinelli, C., and F. Galdiero.** 1967. Ion-binding properties of cell wall of *Staphylococcus aureus*. Riv. Biol. (Perugia) **60**:297–305.
14. **Degens, E. T., and V. I. Ittekkot.** 1981. *In situ* metal-staining of biological membranes in sediments. Nature (London) **298**:262–264.
15. **Degens, E. T., S. W. Watson, and C. C. Remsen.** 1970. Fossil membranes and cell wall fragments from a 7000-year-old Black Sea sediment. Science **168**:1207–1208.
16. **Doyle, R. J., T. A. Matthews, and U. N. Streips.** 1980. Chemical basis for selectivity of metal ions by the *Bacillus subtilis* cell wall. J. Bacteriol. **143**:471–480.
17. **Eglinton, G., and P. J. Barnes.** 1977. Organic matter in aquatic sediments, p. 25–46. *In* W. E. Krumbein (ed.), Environmental biogeochemistry and geomicrobiology, Vol. 1. Ann Arbor Science Publishers, Inc., Ann Arbor, Mich.
18. **Eglinton, G., P. M. Scott, T. Belsky, A. L. Burlingame, and M. Calvin.** 1964. Hydrocarbons of biological origin from a one-billion-year-old sediment. Science **145**:263–264.
19. **Fyfe, W. S.** 1979. The geochemical cycle of uranium. Philos. Trans. R. Soc. London Ser. A **291**:433–445.
20. **Henderson, M. E. K., and R. B. Duff.** 1963. The release of metallic and silicate ions from minerals, rocks, and soils by fungal activity. J. Soil Sci. **14**:236–246.
21. **Hodge, V. F., M. Koide, and E. D. Goldberg.** 1979. Particulate uranium, plutonium and polonium in biogeochemistries of coastal zone. Nature (London) **277**:206–209.
22. **Krumbein, W. C., and R. M. Garrels.** 1952. Origin and classification of chemical sediments in terms of pH and oxidation-reduction potentials. J. Geol. **60**:1–33.
23. **Lambert, P. A., I. C. Hancock, and J. Baddiley.** 1975. The interaction of magnesium ions with teichoic acid. Biochem. J. **149**:519–524.

24. **Love, L. G., and C. G. Amstutz.** 1966. Review of microscopic pyrite. Fortschr. Mineral. **43**:273–309.
25. **Manchee, R.** 1979. Microbial mining. Trends Biochem. Sci. **4**:77–80.
26. **Mangini, A., C. Sonntag, G. Bertsch, and E. Müller.** 1979. Evidence for a higher natural uranium content in the world rivers. Nature (London) **278**:337–339.
27. **Marquis, R. E., K. Mayzel, and E. L. Carstensen.** 1976. Cation exchange in cell walls of Gram-positive bacteria. Can. J. Microbiol. **22**:975–982.
28. **McConnell, D.** 1979. Biogeochemistry of phosphate minerals, p. 163–204. *In* P. A. Trudinger and D. J. Swaine (ed.), Biogeochemical cycling of mineral-forming elements. Elsevier/North-Holland Publishing Co., New York.
29. **Nissenbaum, A., and D. J. Swaine.** 1976. Organic matter-metal interactions in recent sediments: the role of humic substances. Geochim. Cosmochim. Acta **40**:809–816.
30. **O'Brien, G. W., J. R. Harris, A. R. Milnes, and H. H. Veeh.** 1982. Bacterial origin of east Australian continental margin phosphorites. Nature (London) **294**:442–444.
31. **Pflug, H. D., and H. Jaeschke-Boyer.** 1979. Combined structural and chemical analysis of 3,800-million-year-old microfossils. Nature (London) **280**:483–486.
32. **Pierce, D., and P. Cloud.** 1979. New microbial fossils from 1.3 billion-year-old rock of Eastern California. Geomicrobiol. J. **1**:295–309.
33. **Pluman, I. I.** 1971. Uranium contents in the upper Jurassic black argillites of the West Siberian Plate as criterion of geochemical conditions of sedimentation. Geochem. Int. **8**:716–721.
34. **Roedder, E.** 1982. Are the 3,800-M yr-old Isua objects microfossils, limonite-stained fluid inclusions, or neither? Nature (London) **293**:459–462.
35. **Rogers, S. R., and J. J. Anderson.** 1976. Measurement of growth and iron deposition in *Sphaerotilus discophorus*. J. Bacteriol. **126**:257–263.
36. **Tabushi, I., Y. Kobuke, and T. Nishiya.** 1979. Extraction of uranium from sea water by polymer-bound macrocyclic hexaketone. Nature (London) **280**:665–666.
37. **Timperley, M. H., and R. J. Allan.** 1974. The formation and detection of metal dispersion haloes in organic late sediments. J. Geochem. Explor. **3**:167–190.
38. **Tooms, J. S., C. P. Summerhayes, and D. S. Cronan.** 1969. Geochemistry of marine phosphates and manganese deposits. Oceanogr. Mar. Biol. Annu. Rev. **7**:49–100.
39. **Vine, J. D., and E. B. Tourtelot.** 1970. Geochemistry of black shale deposits: a summary report. Econ. Geol. **65**:253–272.
40. **Youssef, M. I.** 1965. Genesis of bedded phosphates. Econ. Geol. **60**:590–600.